

A TWO-DIMENSIONAL FLOW MODEL FOR THE PROCESS SIMULATION OF COMPLEX SHAPE COMPOSITE LAMINATES

PASCAL HUBERT, REZA VAZIRI* AND ANOUSH POURSAITIP

*Composites Group, Departments of Metals and Materials Engineering and Civil Engineering,
The University of British Columbia, Vancouver, B.C., Canada, V6T 1Z4*

ABSTRACT

A numerical flow-compaction model is developed and implemented in a finite element code to simulate the multiple physical phenomena involved during the autoclave processing of fibre-reinforced composite laminates. The model is based on the effective stress formulation coupled with a Darcian flow theory. A Galerkin approach is employed to discretize the weak form of the governing equations. The current formulation successfully describes the compaction behaviour of complex shape laminates caused by flow of the resin. A parametric study is performed to investigate the effect of the material properties on the compaction of angle-shaped composite laminates. It is found that the fibre bed shear modulus significantly affects the compaction behaviour in the corner sections of curved laminates while the resin viscosity and fibre bed permeability affect the compaction rate of the laminate. Copyright © 1999 John Wiley & Sons, Ltd.

KEY WORDS: composites; modelling; processing; flow; compaction

1. INTRODUCTION

Modelling the autoclave processing of composite materials has been the focus of an increasing number of research articles over the last 20 years (for example, see the review article by Hubert and Poursartip¹). The ultimate goal of process modelling is to predict the curing behaviour of large and complex structures. Because of the complexity and variety of mechanisms occurring during processing (such as heat transfer, flow, compaction, resin cure and stress development), it is a daunting task to model the processing of complex structures in a monolithic model. To overcome this difficulty, a modular approach is typically employed for the overall process model structure.^{2,3} As illustrated in Figure 1, the main body of such a process model consists of a series of 'modules', each responsible for performing a single task such as calculating resin flow (the 'flow-compaction' module) or development of internal stresses (the 'stress-deformation' module).

* Correspondence to: Reza Vaziri, Department of Civil Engineering, The University of British Columbia, 2324 Main Mall, Vancouver B.C., Canada V6T 1Z4. E-mail: reza.vaziri@ubc.ca

Contract/grant sponsor: Natural Sciences and Engineering Research Council of Canada

CCC 0029–5981/99/010001–26\$17.50
Copyright © 1999 John Wiley & Sons, Ltd.

*Received 9 July 1997
Revised 25 March 1998*

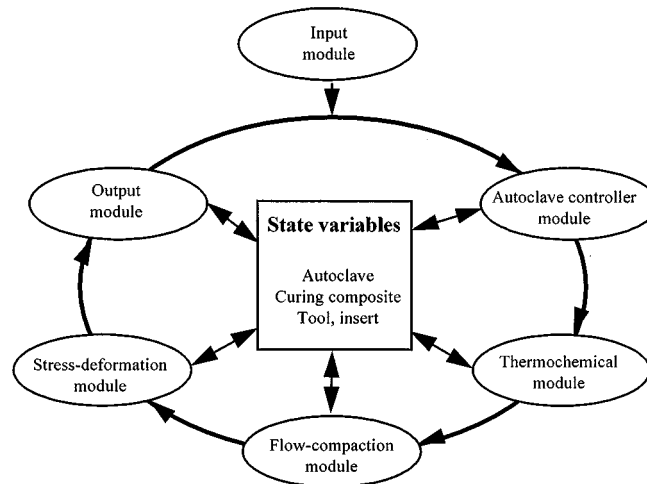


Figure 1. Processing model flowchart showing the different modules (from Hubert *et al.*³)

The various modules are called as needed by a controlling routine as the solution marches forward in time. At the beginning of each time step, an ‘autoclave controller’ module, simulating automated autoclave control, updates all process variables including the autoclave air temperature, the autoclave pressure and the vacuum bag pressure. A central database which contains a description of the modelled components (such as composite, tool, inserts, etc.) is updated by each solution module as they are called. A complete description of the implementation of this approach has been provided by Hubert *et al.*³ In this paper, we focus our attention on the specifics of the development of the module dealing with the flow and compaction behaviour of composites.

Resin flow is an important phenomenon since it affects the fibre volume fraction distribution, the mechanical properties of the laminate and the final dimension of the part. The modelling of resin flow during processing for thermoset matrix composites has been reviewed extensively in Reference 1. Traditionally, the flow equations have been solved numerically by using the finite difference technique.^{2,4–6} This method is convenient for simple geometries such as flat laminates. However, the governing equations have to be solved using the finite element method when dealing with complex structures. For soil consolidation problems, this method has been applied successfully.^{7,8} In thermoset matrix composite manufacturing, the flow of resin has been previously modelled using finite elements in resin transfer moulding process^{9,10} and in autoclave processing.¹¹ Processing of thermoplastic matrix composites has also been modelled using the finite element technique.^{12,13}

A compaction-flow model for flow through a porous medium is available in the commercial code ABAQUS¹⁴ to model consolidation of granular solids. Attempts were made to use this code to solve the present problem. Unfortunately, special features such as variable viscosity and a general fibre bed constitutive law are not implemented in ABAQUS. Therefore, a new special purpose finite element code was developed for the purposes of this study. The process model developed is incorporated in a finite element code called COMPRO.¹⁵ This paper presents the

formulation used for the flow-compaction module. A parametric study of the more important parameters for the flow-compaction model will also be presented.

2. MODEL DEVELOPMENT

2.1. Assumptions

Performing the analysis on only a 2-D section (Figure 2) is believed to be adequate and appropriate for many composite structures, as at least one dimension is usually much larger than the other two. Gradients in this third direction are correspondingly small and can safely be ignored. The following assumptions are made in the present model:

1. a plane strain condition is assumed to prevail and thus only a slice (cross-section) through the part is discretized
2. the composite material is idealized as a void free fibre bed fully saturated with a curing resin
3. an individual ply is composed of regular, unidirectional, very stiff and incompressible fibres that can be arbitrarily oriented in the plane of the ply (Figure 2)
4. the resin is assumed to behave as an incompressible Newtonian fluid
5. the resin flows relative to the fibre bed
6. the effect of gravity is included
7. the resin viscosity changes with temperature and degree of cure
8. the temperature effects on the physical properties (e.g. density) of the resin and the fibre are not included explicitly in the governing equations, but these properties are updated at the beginning of every time step, based on the appropriate equations^{16,17}
9. spatial variation of the composite porosity are assumed to be negligible.

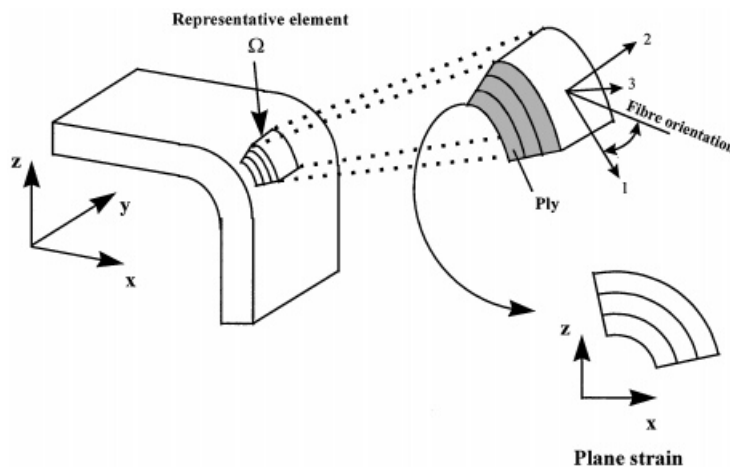


Figure 2. Laminates representative volume and plane strain composite element

2.2. Governing equations

Figure 2 shows the representative element of a curved composite part defining the domain where the governing equations must be satisfied. The governing equations of the system must describe the behaviour of the composite constituents: the fibre bed and the resin. Firstly, the equilibrium of forces on the representative element is considered. Secondly, the mass conservation for the representative element must be satisfied. The following equations were obtained from several references dealing with the consolidation of porous media.^{7,8} For a porous medium saturated with a single phase fluid, the total stress tensor σ_{ij} is separated into two parts as (tensile stresses are considered positive):

$$\sigma_{ij} = \bar{\sigma}_{ij} - \delta_{ij}P \quad (1)$$

where $\bar{\sigma}_{ij}$ is the fibre bed effective stress, δ_{ij} is the Kronecker delta ($\delta_{ij} = 1$ for $i = j$ and $\delta_{ij} = 0$ for $i \neq j$) and P is the resin pressure. For the representative element, the equilibrium equation for a differential element of the composite is

$$(\bar{\sigma}_{ij} - \delta_{ij}P)_{,j} + F_i = 0 \quad (2)$$

The resin flows through the fibre bed according to Darcy's law. Accordingly, the resin velocity v_i relative to the fibre bed is expressed as

$$v_i = -\frac{K_{ij}}{\mu}(P + \rho_R gh)_{,j} \quad (3)$$

where K_{ij} is the fibre bed permeability tensor, μ is the resin viscosity, ρ_R is the resin density, g is the acceleration due to gravity and h is the height above a reference point. For the composite representative element, the conservation of mass is then applied to the fibres and the resin. Considering the assumptions stated previously, the conservation of mass requires

$$(\dot{u}_i)_{,i} + (v_i)_{,i} = 0 \quad (4)$$

where \dot{u}_i is the fibre bed velocity. Combining equations (3) and (4), we obtain the final resin flow continuity equation for the curing composite:

$$(\dot{u}_i)_{,i} = \left(\frac{K_{ij}}{\mu}(P + \rho_R gh)_{,j} \right)_{,i} \quad (5)$$

The continuity equation (5) implies that the volumetric deformations of the composite are caused by the flow of the resin out of the representative element (Figure 2). This implies that the dimensional reference for the composite is in fact the fibre bed dimensions.

2.3. Boundary and initial conditions

The solution to the problem of flow and compaction involves solving a set of transient differential equations subjected to a set of initial conditions and boundary conditions that need to be specified. The state variables that describe the evolution of the flow-compaction process are the fibre bed displacements, u_i and the resin pressure, P . All pertinent parameters can be derived from these primary state variables. The initial and boundary conditions are summarized in Table I.

Table I. Summary of the initial and boundary conditions for the flow-compaction model

Initial conditions, for $t = 0$, in the domain Ω		
$V_f = V_f^0, P = P_{\text{atm}}, \bar{\sigma} = 0$		
Boundary conditions, for $t > 0$, on the surface Γ		
Displacement	External pressure	Flow
Free	$\sigma = f(t)$	Impermeable: $\partial P / \partial n_i = 0$
Fixed: $u_i = 0$		Permeable: $P_b = f(t)$
Sliding*: $u^n = 0$		

* u^n is defined as the displacement normal to the boundary

The initial fibre volume fraction of the composite, V_f^0 , is specified and the initial resin pressure is assumed to be atmospheric and the fibre bed is initially stress-free. Boundary conditions specify the state of displacements, applied pressure and resin pressure at the edge of the laminate. The displacement boundary conditions, which are held constant during the entire solution, are separated into three types: free, fixed and sliding. The sliding condition is obtained by allowing displacement in the direction tangent to the surface boundary. In the case of a surface oriented in an arbitrary orientation, standard co-ordinate transformations are applied to the degrees of freedom affected by the sliding condition.¹⁸ The external pressure can vary during the solution. The flow boundary condition is either impermeable or permeable. A permeable boundary condition is specified by imposing a prescribed resin pressure at that boundary (i.e. 'free flow' boundary condition). The boundary pressure is the pressure of the vacuum bag and can change with time. The impermeability condition is equivalent to having a zero normal pressure gradient at the boundary (i.e. $\partial P / \partial n_i = 0$, where n_i is the unit normal vector to the boundary). The prescribed resin flow flux at the boundary is not considered in the present model. In autoclave processing, the resin flux at the boundary is caused by the imposed resin pressure boundary condition. For other processing methods like resin transfer moulding (RTM), the implementation of prescribed resin flux at the boundary would be required.

2.4. Composite constitutive law

The fibre bed constitutive law relates the fibre bed stresses to the strains that a representative element of a unidirectional composite is subjected to (Figure 3). Cai and Gutowski¹⁹ proposed a constitutive law for a fibre bundle where the stresses were divided into normal and deviatoric shear components. The normal stresses result in the elastic response of the material while the shear stresses are responsible for the viscous flow. In their work, they ignored the viscous shear response of the material claiming that for the case of autoclave processing the shear deformations are negligible. Thus, for a plane strain problem their constitutive law can be written as

$$\begin{Bmatrix} \bar{\sigma}_1 \\ \bar{\sigma}_3 \end{Bmatrix} = \begin{bmatrix} E_1 & E_{13} \\ E_{31} & E_3 \end{bmatrix} \begin{Bmatrix} \varepsilon_1 \\ \varepsilon_3 \end{Bmatrix} \quad (6)$$

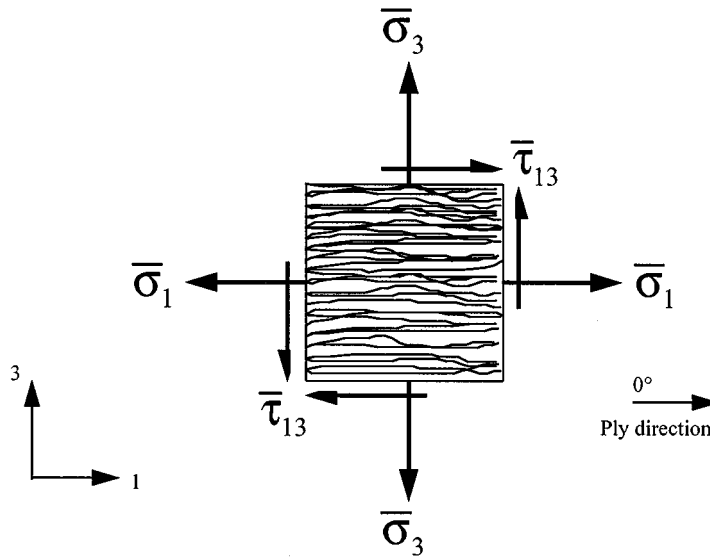


Figure 3. Stress state on a representative element of a unidirectional ply

where $\bar{\sigma}_1$, $\bar{\sigma}_3$ and ε_1 , ε_3 are the stresses and strains (Figure 3), and E_1 , E_{13} , E_{31} and E_3 are the fibre bundle elastic constants. For an element of a unidirectional fibre bundle, all elastic constants are functions of both the fibre bed state and fibre volume fraction. In soil mechanics problems,⁷ the porous medium is assumed to be isotropic. In this case, the shear response is taken to be elastic and coupling is also included.

For the present model, a constitutive law that includes elements of both of these approaches is adopted. A simplified model is employed because there is a lack of experimental evidence to support a more complex constitutive law. Consequently, the present compaction model is based on the following rate-independent elastic constitutive relation:

$$\begin{Bmatrix} \bar{\sigma}_1 \\ \bar{\sigma}_3 \\ \bar{\tau}_{13} \end{Bmatrix} = \begin{bmatrix} E_1 & 0 & 0 \\ 0 & E_3 & 0 \\ 0 & 0 & G_{13} \end{bmatrix} \begin{Bmatrix} \varepsilon_1 \\ \varepsilon_3 \\ \gamma_{13} \end{Bmatrix} \quad (7)$$

where E_1 , E_3 and G_{13} are the elastic constants describing the fibre bundle compaction behaviour. In equation (7), the coupling between the longitudinal and transverse response has been neglected. Using equations (40) and (42) in Reference 19, it can be shown that for the current application, E_{13} and E_{31} in equation (6) are very small, and therefore can be neglected.

Since the fibres are oriented in the longitudinal direction, E_1 is assumed to be a function of the fibre longitudinal elastic modulus and the fibre volume fraction. E_3 varies with the fibre bundle transverse strain, and is calculated from the experimentally obtained fibre bed compaction curve. G_{13} , is a material property that has not been considered previously in composites process modelling work, since the primary focus has been flat laminates. However, when considering shaped parts, some measure of shear behaviour, namely G_{13} needs to be included. It will be

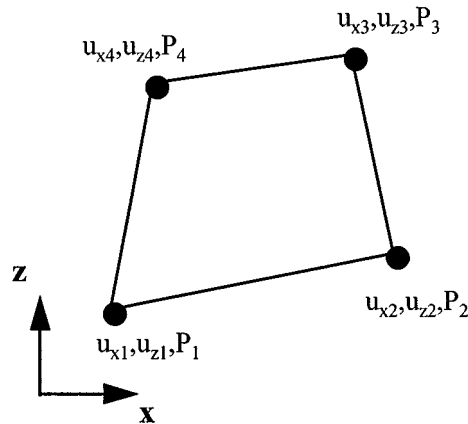


Figure 4. Bilinear quadrilateral element and degrees of freedom (i.e. displacements u_{xn} , u_{zn} and pressure P_n where n is the node number)

demonstrated later that the inclusion of the shear term is very important for shapes that are not flat.

2.5. Finite element formulation

The governing equations (2) and (5) form a system of differential equations that have to be discretized into a system of algebraic equations using the weighted residual method. The Galerkin method, which is the most popular weighted residual method, is used to arrive at the finite element equations for the present model. Most of the following developments are based on standard finite element procedures that are well documented.^{18,20}

The domain is discretized with bilinear quadrilateral isoparametric elements (Figure 4). Most laminates can be meshed using quadrilateral elements. The choice of an isoparametric element enables one to apply the equations to a domain of arbitrary shape in the x - z plane. For coupled fluid flow-elasticity problems, it is recommended to use an eight-noded rectangular element with quadratic shape functions for the displacements and linear shape functions for the pressure.^{7,20} Although the problem has been successfully solved using four-noded bilinear elements,^{21,22} the eight-noded elements reduce some numerical instabilities arising from the coupling of the governing equations.²³ For simplicity and computational efficiency, the bilinear four-noded element with pressure and displacement degrees of freedom at each node is adopted here.

Different options are available for solving the governing equations. One can uncouple the system of equations by separately solving the stress equilibrium and then the continuity (or fluid flow) equation. This technique has been used in the majority of flow-compaction models for composites.⁶ Typically, for soil mechanics applications, the solution is applied to the coupled system of equations,⁷ although an uncoupled solution scheme has been developed by Zienkiewicz. *et al.*²⁴ For the present model, the coupling approach is used even though the problem can be assumed quasi-static and hence the uncoupled method would be justified.

The system of algebraic equations in this case can be written as:

$$\begin{bmatrix} \mathbf{S} & \mathbf{L} \\ \mathbf{0} & \mathbf{H} \end{bmatrix} \begin{bmatrix} \mathbf{a}^u \\ \mathbf{a}^p \end{bmatrix} + \begin{bmatrix} \mathbf{0} & \mathbf{0} \\ \mathbf{L}^T & \mathbf{0} \end{bmatrix} \begin{bmatrix} \dot{\mathbf{a}}^u \\ \dot{\mathbf{a}}^p \end{bmatrix} = \begin{bmatrix} \mathbf{F}^s \\ \mathbf{F}^f \end{bmatrix} \quad (8)$$

where

$$\mathbf{S} = \int_{\Omega} \mathbf{B}^T \mathbf{D}_T \mathbf{B} \, d\Omega \quad (9)$$

$$\mathbf{L} = - \int_{\Omega} \mathbf{B}^T \delta \mathbf{N} \, d\Omega \quad (10)$$

$$\mathbf{H} = - \int_{\Omega} \mathbf{G}^T \frac{\mathbf{K}}{\mu} \mathbf{G} \, d\Omega \quad (11)$$

$$\mathbf{F}^s = \int_{\Omega} \mathbf{N}^T \mathbf{F}^g \, d\Omega + \int_{\Gamma} \mathbf{N}^T \sigma^n \, d\Gamma \quad (12)$$

$$\mathbf{F}^f = \int_{\Omega} \mathbf{G}^T \mathbf{H}^d \, d\Omega \quad (13)$$

$$\mathbf{G} = \nabla \mathbf{N}^T = \left[\frac{\partial \mathbf{N}}{\partial x} \quad \frac{\partial \mathbf{N}}{\partial z} \right]^T \quad (14)$$

where \mathbf{a}^u and \mathbf{a}^p are the vectors of displacement and pressure variables, \mathbf{D}_T is the tangent material stiffness matrix for the fibre bed, \mathbf{F}^g is a vector of gravitational forces per unit volume, δ is a row vector defined as $\delta = \{1, 1, 0\}$, \mathbf{N} is a column vector of the bilinear shape functions, \mathbf{B} is the standard strain–displacement matrix, \mathbf{H}^d is a matrix containing the piezometric pressure term and σ^n is a vector containing the boundary stresses.

The element domain integrals and the boundary integrals (equations (9)–(13)) are evaluated numerically using the Gaussian quadrature technique. Applying the appropriate essential boundary conditions (i.e. displacements and resin pressure), equation (8) is then solved for the unknown nodal variables. Apart from the standard spatial integrations, the solution of the system of equations requires two other fundamental solution strategies. The presence of a time derivative in equation (8) implies that the governing equations have to be integrated in time. Finally, because of the non-linear behaviour of the fibre bed elasticity and permeability, a non-linear iterative technique is required.

The consolidation is a transient problem and the system of equations has to be integrated in time. The system of ordinary differential equations (equation (8)) can be rewritten as follows:

$$\mathbf{C}\dot{\mathbf{U}} + \mathbf{D}\mathbf{U} = \mathbf{F} \quad (15)$$

where \mathbf{U} is the vector of unknown nodal variables, $\dot{\mathbf{U}}$ is the vector of time derivatives of the unknown nodal variables, \mathbf{C} is the damping matrix, \mathbf{D} is the stiffness matrix and \mathbf{F} is the load vector. The system of equations is of first order in time and a number of methods are available for its integration with the direct Euler integration methods being the most popular. Among them, the implicit Euler method is unconditionally stable but not unconditionally accurate. The advantage of this method is that it is possible to use relatively large time steps. For our problem, the total time scale is long (in the minutes range) and the process is quasi-static, therefore the time

steps are necessarily long. The time integration solution has to be coupled with a non-linear iterative technique since the problem contains material properties that are functions of the nodal variables.

Several iterative solution strategies are available to solve the problem and the choice of a method depends mainly on the type or the severity of the non-linearity. For our problem the non-linearities arise from the resin viscosity, the fibre bed permeability and the fibre bed transverse elasticity. The resin viscosity can be assumed constant during a time step provided that the rate of change of the resin viscosity is small. After each time step, the resin viscosity will be updated based on the actual element temperature and resin degree of cure. For the permeability, a substitution method²⁵ is used where the permeability is updated at every iteration until convergence is reached according to a certain criterion. Finally, for the fibre bed elasticity, a Newton–Raphson technique²⁶ is employed to take into account the severe hardening in the effective stress–strain relationship. The internal load vector is calculated using the following relation:

$$\mathbf{F}^{\text{int}} = \begin{bmatrix} \int_{\Omega} (\mathbf{B}^T \bar{\boldsymbol{\sigma}} + \mathbf{L} \mathbf{a}^p) d\Omega \\ \int_{\Omega} \mathbf{H} \mathbf{a}^p d\Omega \end{bmatrix} \quad (16)$$

where $\bar{\boldsymbol{\sigma}}$ is the actual updated effective stress vector obtained from the constitutive model.

2.6. Model verification

Before applying the flow-compaction model to study complex shapes, a number of verification runs were performed. The purpose of the verification runs was to test the element formulation and implementation. These runs consisted of testing the model at different levels of complexity ranging from simple static cases to the full non-linear transient solution. Several comparison sources were available to validate the present model predictions. In particular, the linear solution for a 1-D consolidation coupled with 1-D flow can be compared with an analytical solution. For the non-linear solution, either ABAQUS or a previously developed 1-D composite processing model, LAMCURE,²⁷ were used. The verification runs were also used to define the limitations of the present model and the level of accuracy of the solution. In all cases, the present finite element model was found to successfully predict the compaction behaviour of an elastic porous medium. The transient non-linear solution algorithm is correctly implemented as shown by comparison of simulation results with closed-form predictions or ABAQUS results (Figures 5 and 6). The present processing model is in good agreement with previously developed models for composite materials (LAMCURE, Figure 7). The small disagreement in the final solution, particularly for the high flow resin system, comes from the fact that the present model uses a small strain formulation as opposed to LAMCURE, which updates the mesh in order to account for geometric non-linearities. However, the present flow-compaction model is suitable for composites that are made up of low flow resin systems. These types of resins are being used widely in the current practical laminated structures that undergo autoclave processing.

3. PARAMETRIC STUDY

A parametric study can have two main goals: to investigate the effect of a parameter on the final model predictions or to study the effect of variation in input parameters that are not defined (or

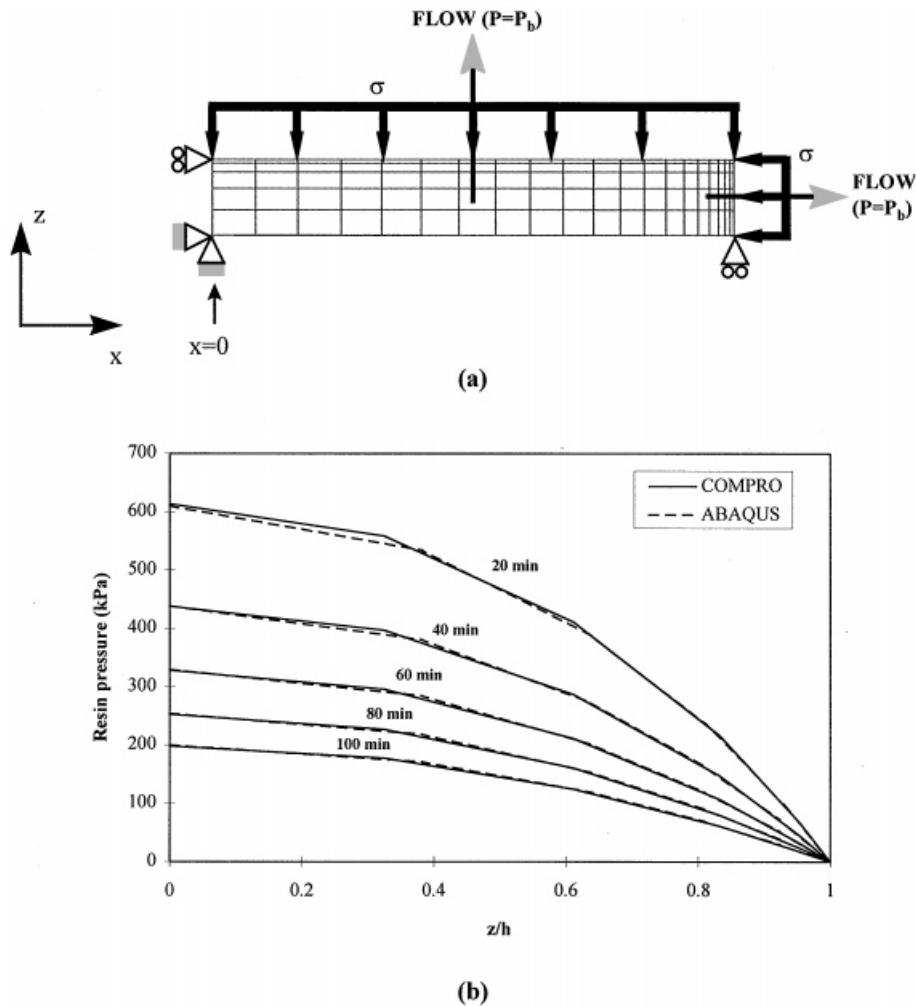


Figure 5. Comparison between predictions by COMPRO versus ABAQUS for a 2-D flow consolidation: (a) boundary conditions for the 100 elements mesh; (b) predicted vertical pressure profile evolution with time at $x = 0$

measured) to a satisfactory level of confidence and accuracy. Parametric studies on flat panels have been conducted by previous researchers with flow-compaction models^{2,4,28} but the modelling of curved shape laminates for autoclave processing has never been addressed.¹ Therefore, the present parametric study focuses on the effect of material properties on the compaction of an L-shaped angle laminate. The following properties are investigated: resin viscosity, fibre bed permeability (longitudinal and transverse) and fibre bed constitutive law (longitudinal, transverse and shear moduli). The resin viscosity and fibre bed transverse modulus are generally characterized to a good level of accuracy.¹ Thus, the effect of only small variations in these properties on the compaction of the laminate is studied. For the fibre bed permeability, the range of the longitudinal and transverse permeabilities is obtained from the literature.¹⁶ Finally, the

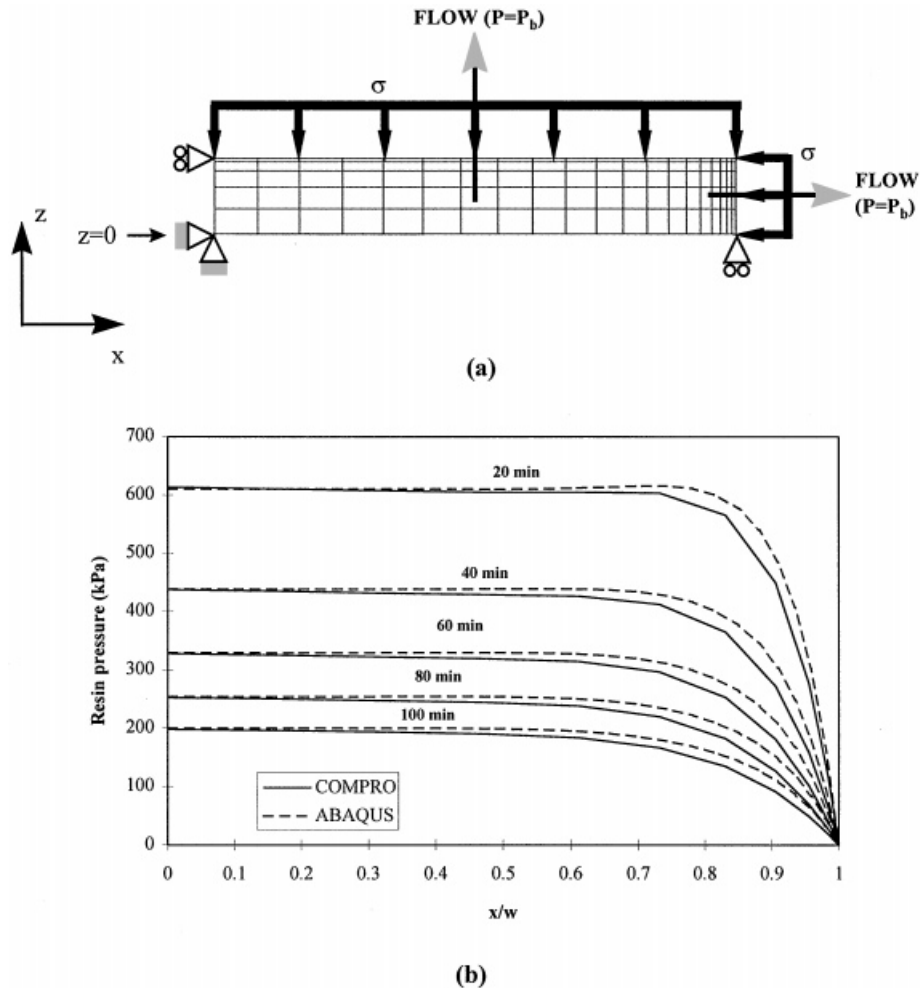


Figure 6. Comparison between predictions by COMPRO versus ABAQUS for a 2-D flow consolidation: (a) boundary conditions for the 100 elements mesh; (b) predicted horizontal pressure profile evolution with time at $z = 0$

fibre bed longitudinal and shear moduli have never been characterized nor has their effect on the compaction behaviour of angle shaped laminates been addressed in the literature. Thus, the parametric study for these parameters covers a wide range to assess their effect.

3.1. Finite element model and runs definition

The laminate geometry selected for the current parametric study is a 90° angle (L-shaped) laminate with a carbon-epoxy material (AS4/3501-6) and unidirectional fibres $[0^\circ]$. The laminate is defined in Figure 8. Assuming symmetry and plane strain conditions ($\epsilon_y = 0$), the finite element mesh represents one half of the laminate as illustrated in Figure 8. The model dimensions and applied boundary conditions are also shown in Figure 8. The autoclave pressure acts on the top

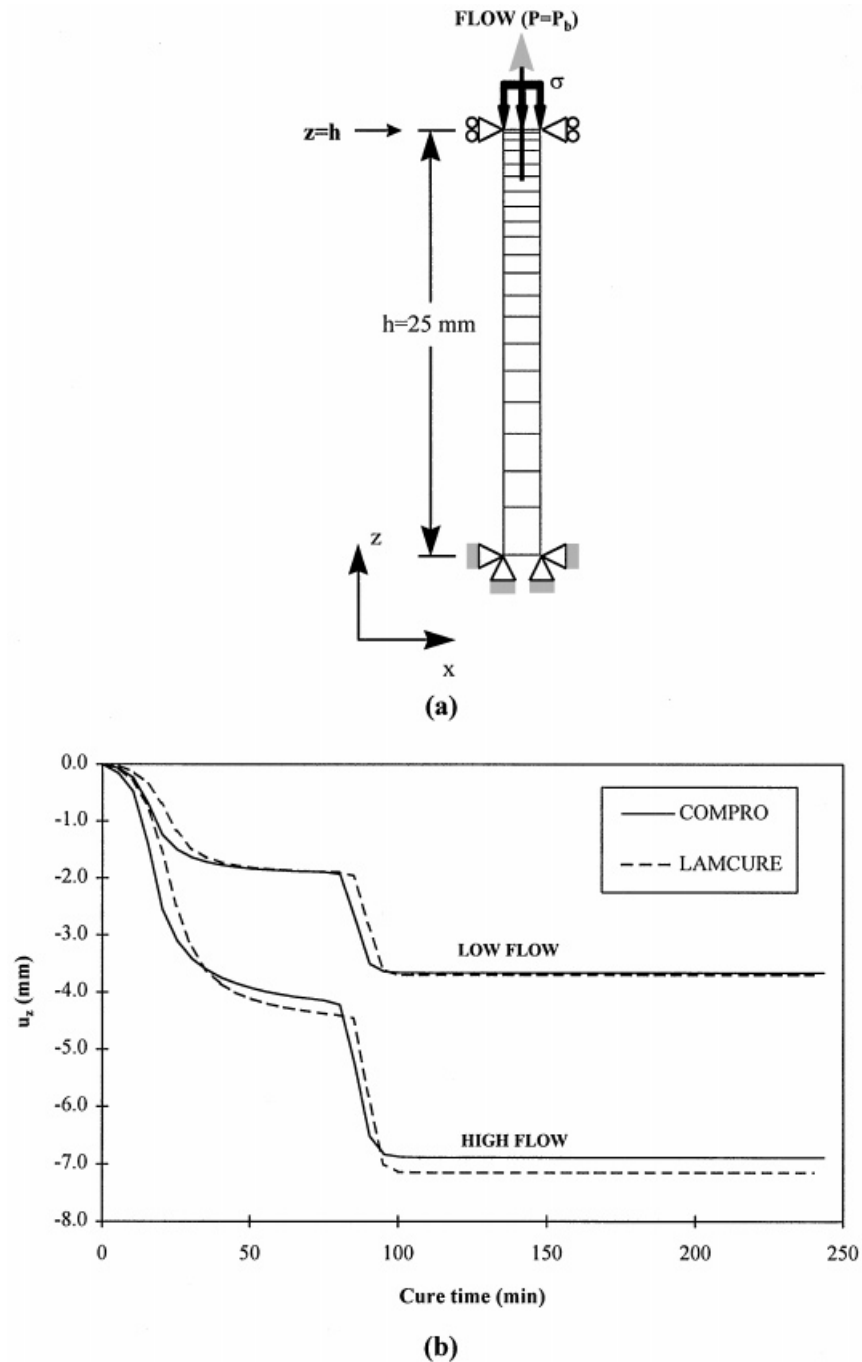


Figure 7. Comparison between predictions by COMPRO versus LAMCURE²⁷ for a 1-D flow consolidation: (a) boundary conditions for the 20 elements mesh; (b) predicted variation of vertical displacement at the top of the model ($z = h$) for both low and high flow systems

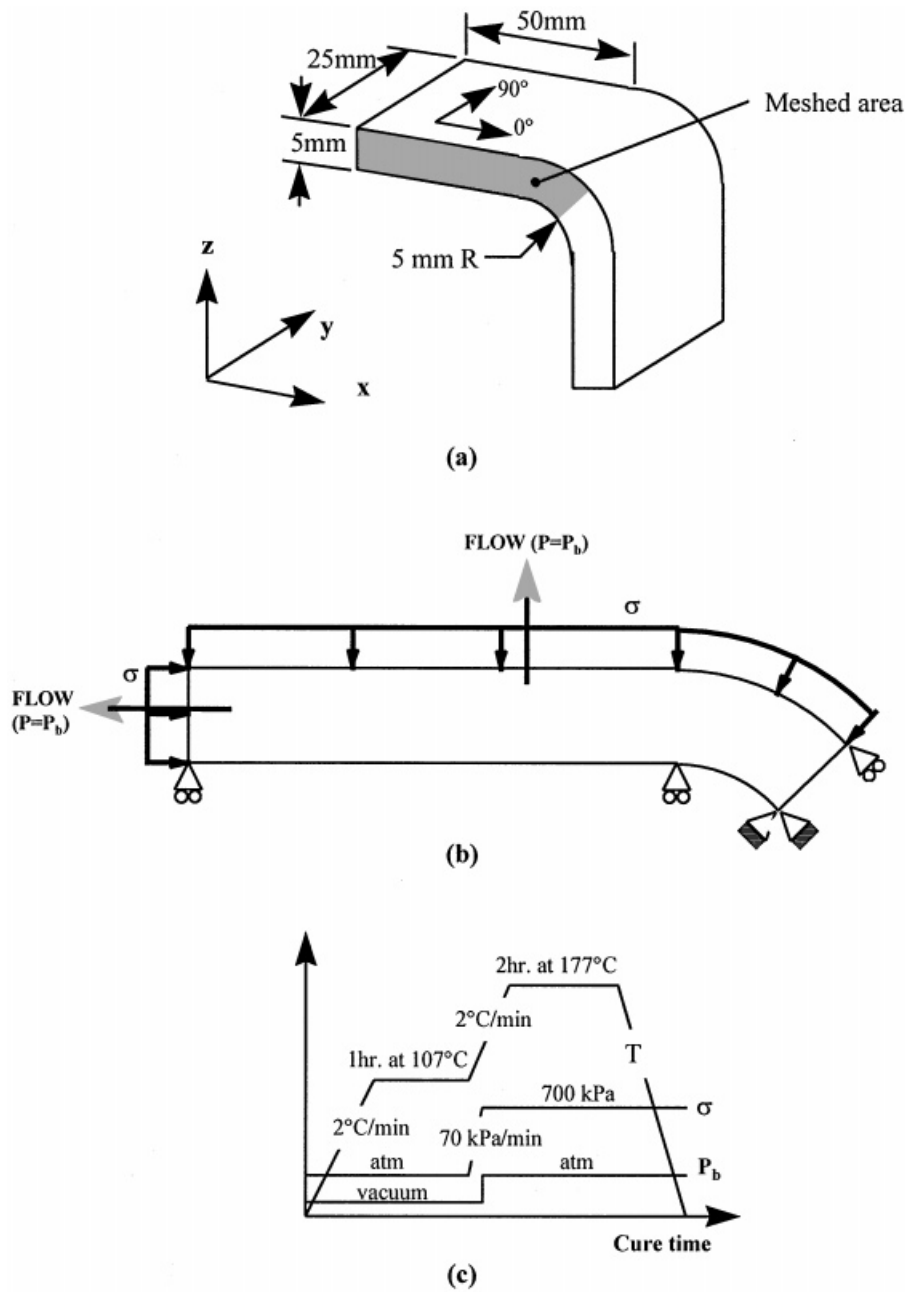


Figure 8. Angle laminate dimensions: (a) and finite element model boundary conditions; (b) and cure cycle input; (c) for the nominal case of the parametric study (SANOM)

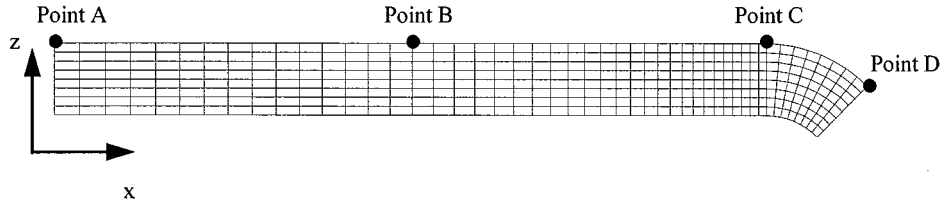


Figure 9. Finite element mesh used for the parametric study. The location for the normal displacement (u_n) outputs is shown

surface and edges of the laminate. Flow of resin is allowed by imposing a boundary resin pressure equal to the bag pressure. The presence of a rigid tool is accounted for by applying a sliding displacement boundary condition at the bottom surface of the laminate. The symmetry boundary condition is imposed at the right edge of the laminate. For the simulations, the laminate surface temperature is assumed to be equal to the air temperature of the autoclave. The cure cycle shown in Figure 8 is used for all the simulations. This is a standard cure cycle suggested by the manufacturer of the composite.

Figure 9 shows the finite element mesh used. A total of 464 elements are used with a constant time step of 1 min. The flow-compaction module activates when the resin viscosity drops under 1000 Pa.s. Figure 9 indicates the location of the nodes where the displacement normal to the surface (u_n) is extracted to obtain the laminate compaction behaviour.

The material properties of AS4/3501-6 for the nominal case (SANOM) are taken from the literature and from characterization tests presented in Reference 16. For the resin viscosity (μ), the following relation is used:

$$\mu = \mu_{\infty} \exp(\kappa\alpha) \exp\left(\frac{U}{RT}\right) \quad (17)$$

where μ_{∞} , U , and κ are constants determined from viscometer data, α and T are the resin degree of cure and temperature. For AS4/3501-6, the constants are $\mu_{\infty} = 4.6 \times 10^{-17}$ Pa.s, $U = 114477$ J/mol, and $\kappa = 14.8$. The longitudinal fibre bed permeability (K_1) is defined by the following relation:²⁸

$$K_1 = \frac{r_f^2 (1 - V_f)^3}{4k V_f^2} \quad (18)$$

where r_f is the fibre radius, k is the Kozeny constant and V_f is the fibre volume constant. For AS4/3501-6, the constants are $r_f = 4 \times 10^{-6}$ m and $k = 0.7$. The transverse fibre bed permeability (K_3) is defined by the following relation:²⁹

$$K_3 = \frac{r_f^2 (\sqrt{V'_a/V_f} - 1)^3}{4k' (\sqrt{V'_a/V_f} + 1)} \quad (19)$$

where k' and V'_a are empirical parameters. For AS4/3501-6, the constants are $r_f = 4 \times 10^{-6}$ m, $k' = 0.2$ and $V'_a = 0.82$. The fibre bed longitudinal modulus (E_1) is based on the longitudinal elastic modulus of the fibres. The fibre bed longitudinal modulus is estimated to be 100 GPa using

the rule of mixture for a fibre volume fraction of approximately 50 per cent (i.e. $E_1 = 0.5E$ where $E = 200$ GPa is the fibre longitudinal modulus). The fibre bed shear modulus (G_{13}) is set at 1 MPa for the nominal case. This value is derived from the average fibre bed transverse modulus calculated from the compaction curve for AS4/3501-6. In the pressure range of the analysis (i.e. 0-700 kPa), the average transverse modulus is approximately 2 MPa. Thus, the estimated shear modulus is set to one-half of the transverse modulus. Finally, the instantaneous fibre bed transverse modulus (E_3) is calculated from the fibre bed stress-strain curve measured for AS4/3501-6, presented in Figure 10.

The different resin viscosity profiles (SAVIS1, SAVIS2 and SAVIS3) were obtained by setting a different resin initial degree of cure (α_0) or by using different values of constants (μ_∞ and κ) for the viscosity relation (equation (17)). The range of variation in the fibre bed permeability was obtained by changing the value of the permeability model constants or by using a different permeability model. An increase in the longitudinal permeability (run SAPER1) is obtained by setting $k = 0.35$ in equation (18). A reduction in the longitudinal permeability (run SAPER2) is obtained by using the following relation:³⁰

$$K_1 = \frac{8r_f^2}{c} \frac{(1 - V_f)^3}{V_f^2} \quad (20)$$

with $r_f = 4 \times 10^{-6}$ m and $c = 57$. An increase in the transverse permeability (run SAPER3) is obtained by setting $k = 6$ in equation (18). A reduction in the transverse permeability (run SAPER4) is obtained by setting $V_a' = 0.76$ in equation (19).

The fibre bed longitudinal modulus is varied from a high value of 200 GPa (SAE11) to a low value of 1 GPa (SAE12). The fibre bed shear modulus is varied from a high value of 10 MPa

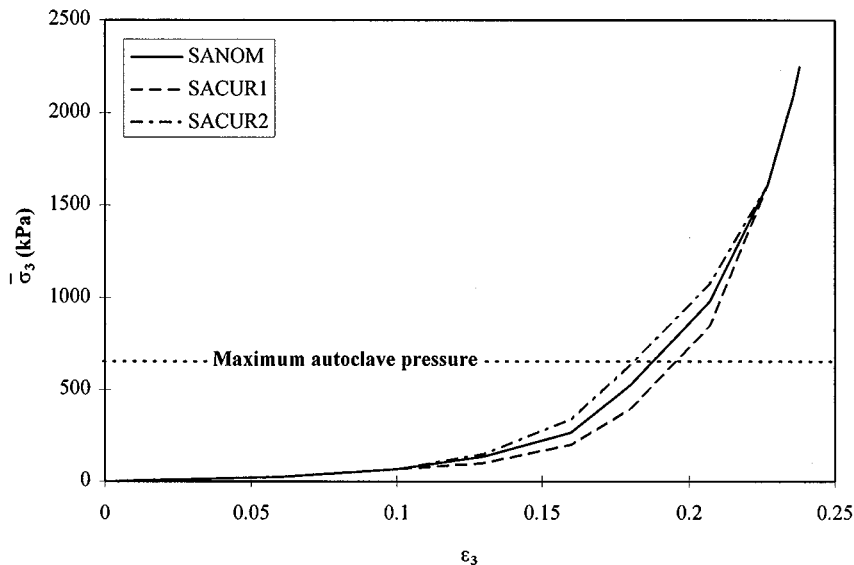


Figure 10. Compaction curves used for the parametric study to investigate the effect of shifting the fibre bed effective stress in the stiffening region ($0.1 < \varepsilon_3 < 0.25$)

(SAG131) to a low value of 10 kPa (SAG132). The change of E_3 is obtained by changing the shape of the compaction curve in the transition region from a low fibre bed modulus to the final very high modulus ($0.1 < \varepsilon_3 < 0.25$). The lower curve (SACUR1) and higher curve (SACUR2) are compared with the nominal case in Figure 10.

3.2. Results and discussion of the parametric study

Table II summarizes the results from the parametric study. The compaction time and the thickness change in the flat section and at the corner of the laminate are shown. As expected, a change of the resin viscosity or the fibre bed permeability affects the time to full compaction but not the final thickness of the laminate. On the other hand, the variation of the parameters of the constitutive law influences the final laminate thickness but not the time to full compaction. Similar results were obtained by Smith and Poursartip.⁶

Table II. Run definition and results for the parametric study

Run	Parameter	Result		
		Time to full compaction (min)	Thickness change in flat section (mm)	Thickness change at corner (mm)
Nominal case				
SANOM	See Figure 8 and text	135	-0.95	-0.52
Resin viscosity				
SAVIS1	$\alpha_0 = 0.1$ (equation (17))	140 (+5)	-0.95 (0)	-0.52 (0)
SAVIS2	$\mu_\infty = 3.5 \times 10^{-17}$ Pa s (equation (17))	135 (0)	-0.95 (0)	-0.52 (0)
SAVIS3	$\kappa = 18$ (equation (17))	150 (+15)	-0.95 (0)	-0.52 (0)
Fibre bed longitudinal permeability				
SAPER1	$k = 0.35$ (equation (18))	135 (0)	-0.95 (0)	-0.52 (0)
SAPER2	$c = 57$ (equation (20))	140 (+5)	-0.95 (0)	-0.52 (0)
Fibre bed transverse permeability				
SAPER3	$k = 6$ (equation (18))	125 (-10)	-0.95 (0)	-0.52 (0)
SAPER4	$k' = 0.2, V'_a = 0.76$ (equation (19))	145 (+10)	-0.95 (0)	-0.52 (0)
Fibre bed compaction curve shape				
SACUR1	See Figure 10	135 (0)	-0.99 (-0.04)	-0.52 (0)
SACUR2	See Figure 10	135 (0)	-0.91 (+0.04)	-0.52 (0)
Fibre bed longitudinal modulus				
SAE11	$E_1 = 200$ GPa	135 (0)	-0.95 (0)	-0.52 (0)
SAE12	$E_1 = 1$ GPa	135 (0)	-0.95 (0)	-0.70 (-0.18)
Fibre bed shear modulus				
SAG131	$G_{13} = 10$ MPa	130 (-5)	-0.95 (0)	-0.05 (+0.47)
SAG132	$G_{13} = 10$ kPa	135 (0)	-0.95 (0)	-0.95 (-0.43)

Note: Value in parentheses represents the variation from the nominal case

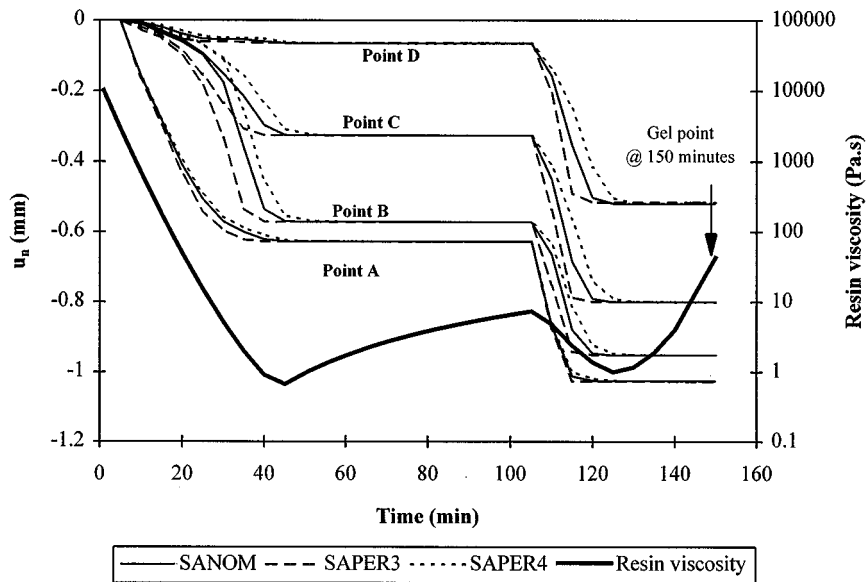


Figure 11. Effect of the variation of the transverse permeability on the angle compaction behaviour. The viscosity profile is also shown indicating the gelation time of the resin

Figure 11 illustrates this result with the effect of a change in K_2 on the laminate compaction. As reported by Loos and Springer,² the processing conditions must be selected such that full compaction of the laminate is achieved before gelation of the resin. For the case studied here, the laminate compacts before the onset of gelation of the resin, as shown in Figure 11. However, under different circumstances, a change in the resin viscosity and the fibre bed permeability could have a significant effect. These issues were discussed in detail in previous work.^{2,6,28,31}

The effect of the shape of the compaction curve on the laminate thickness is presented in Figure 12. The laminate final thickness is affected when the laminate strains normal to the tool are in the range of the compaction curve variation ($0.10 < \epsilon_3 < 0.25$) in Figure 10. Therefore, the final thickness of the flat section, where the strains are large (Points A, B and C, $0.16 < \epsilon_3 < 0.19$), is significantly affected while the final thickness at the corner, where the strains are low (Point D, $\epsilon_3 < 0.10$), is not affected. These results stress the importance of an accurate measurement of the entire fibre bed compaction curve.

The effect of the fibre bed longitudinal modulus is presented in Figure 13. Increasing E_1 has no effect, while decreasing E_1 allows more tangential deformation, which increases the ability of the corner to compact (Point D deformation increases for SAE12). The effect of the fibre bed shear modulus is presented in Figure 14. The variation of G_{13} has a significant effect, particularly at the corner (Point D) and in the transition area between the flat and the corner section (Point C). This is best shown in Figure 15 where the final shapes predicted by the various simulations are compared. A low value for G_{13} (SAG132) leads to a laminate with a constant thickness allowing the corner section to reach full compaction. A high value for G_{13} (SAG131) decreases the ability of the corner to compact.

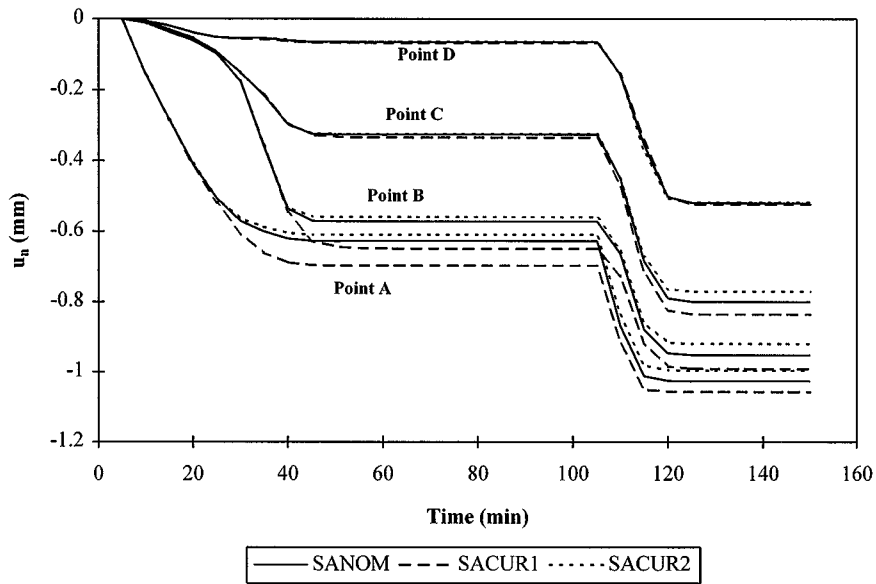


Figure 12. Effect of the compaction curve shape on the angle compaction behaviour

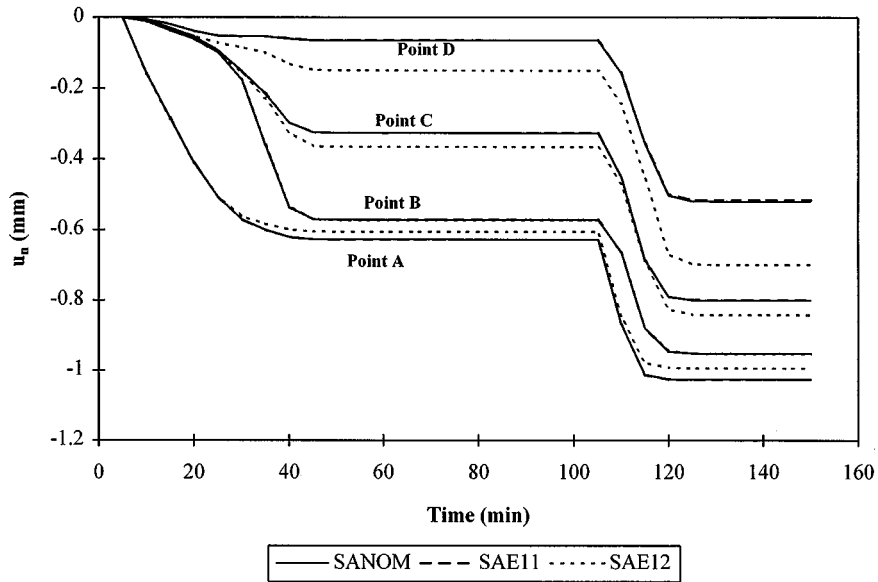


Figure 13. Effect of the fibre bed longitudinal modulus (E_1) on the angle compaction behaviour

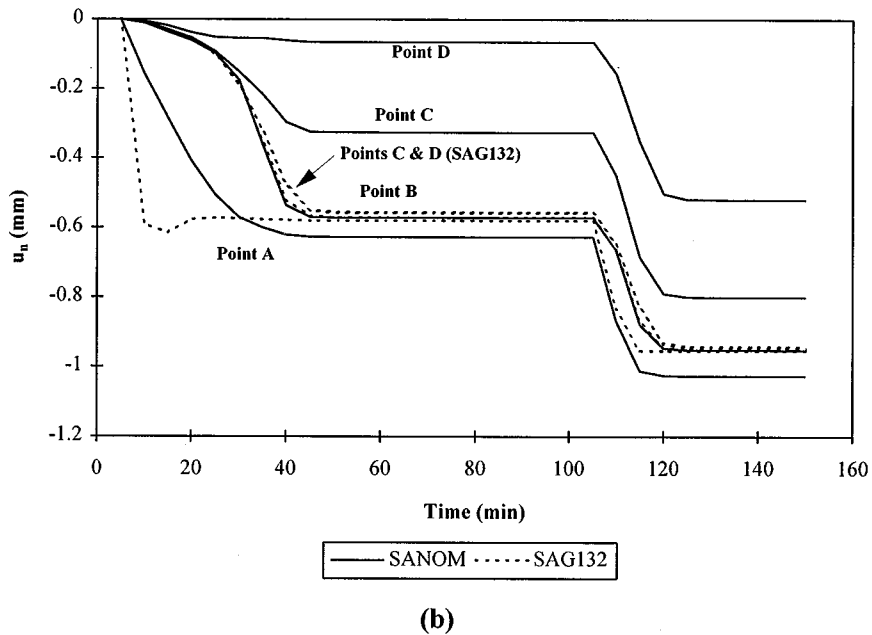
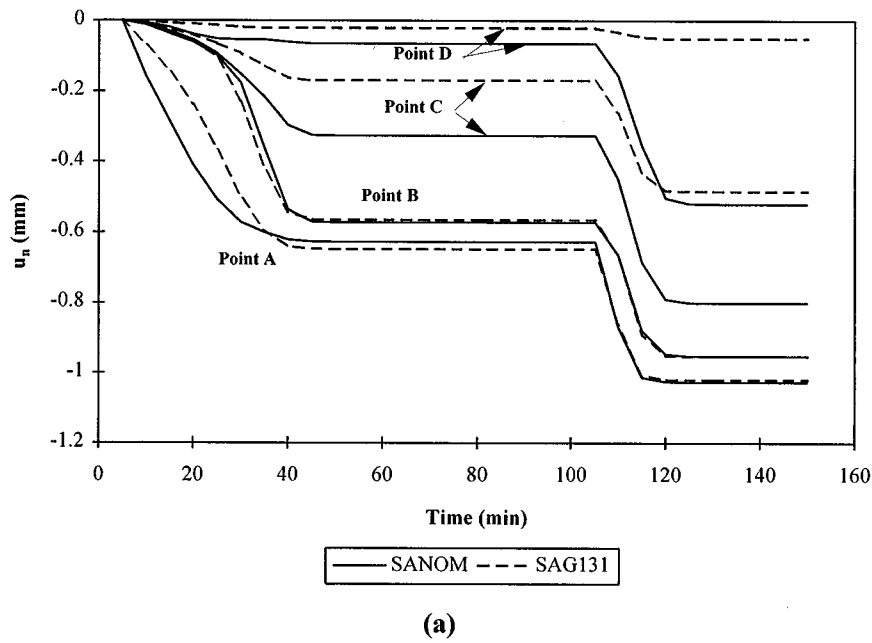


Figure 14. Effect of the fibre bed shear modulus (G_{13}) on the angle compaction behaviour: (a) increase in G_{13} ; (b) decrease in G_{13}

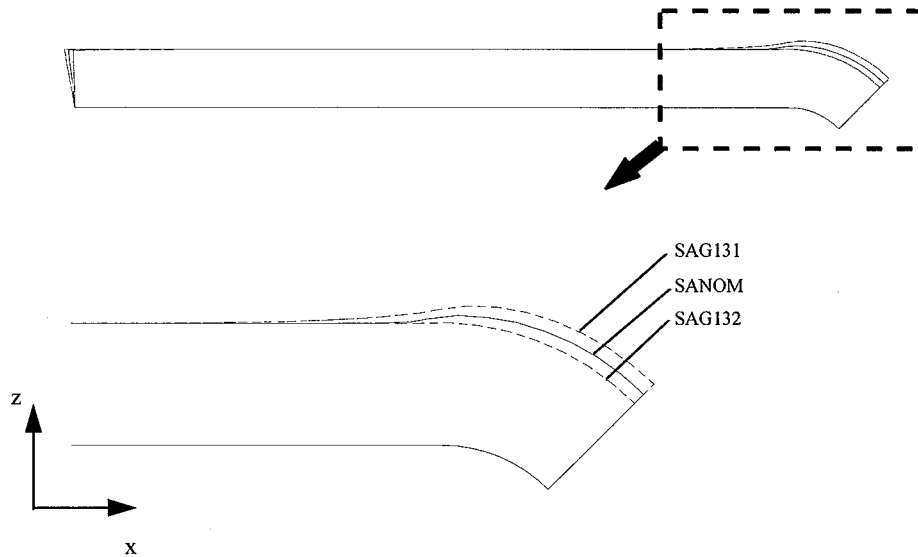
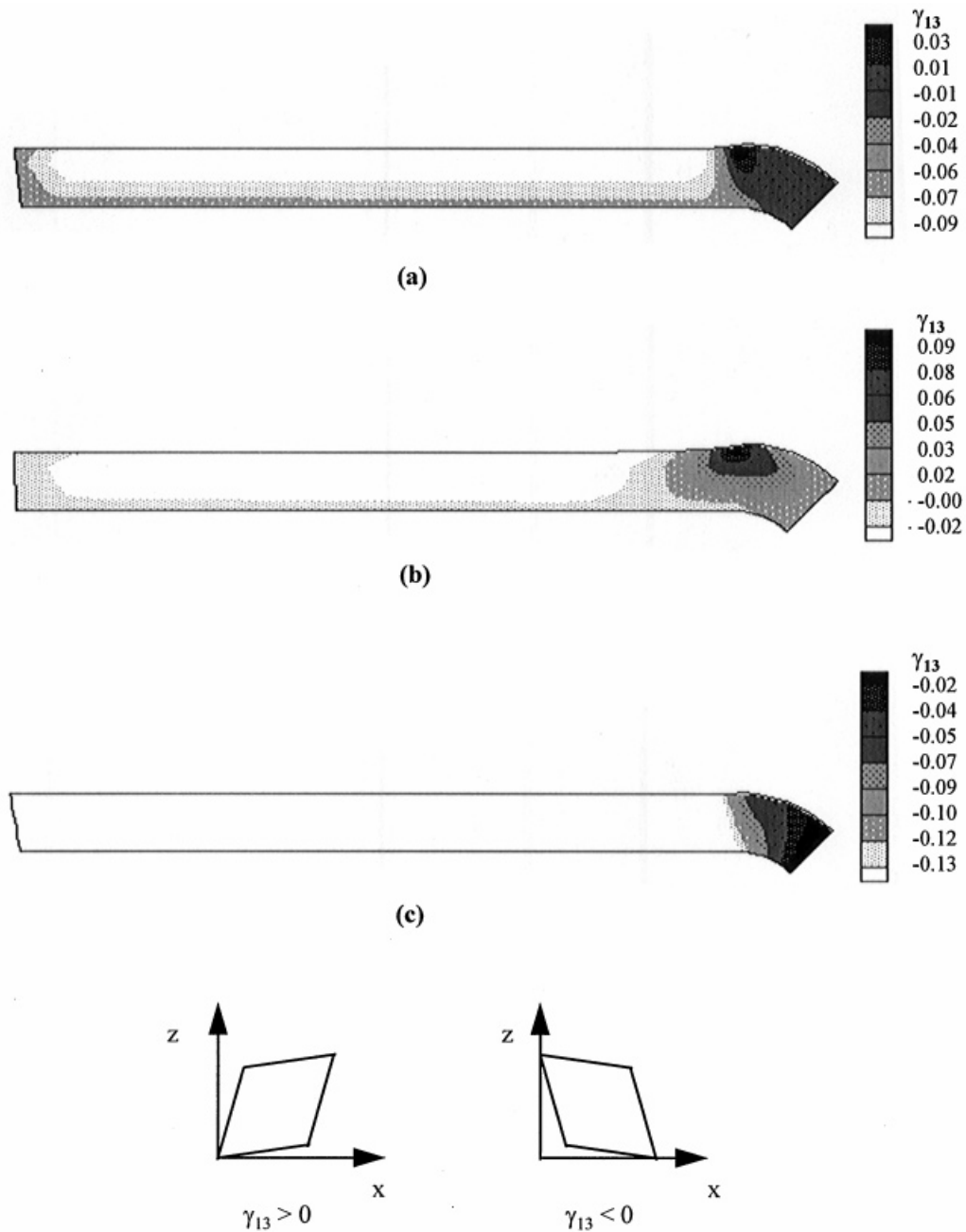


Figure 15. Effect of the fibre bed shear modulus (G_{13}) on the final shape of the angle. The deformation behaviour at the corner is enlarged

A comparison of the fibre bed shear strain (γ_{13}) distributions for the different simulations is shown in Figure 16. For all cases, the negative strains in the flat section are caused by the shearing induced by the action of the fibre bed being pushed away from the corner. The positive shear deformation at the corner (SANOM and SAG131) is caused by the difference in the normal compaction between the flat section and the corner. A variation of G_{13} directly influences the magnitude of the shear deformation as shown in Figure 16. Decreasing G_{13} (SAG132) increases the ability of the fibre bed to shear as indicated by an increase in the maximum shear strain, while increasing G_{13} (SAG131) has the opposite effect. The actual value of G_{13} is unknown, thus the values for the parametric study were chosen to highlight the importance of the fibre bed shear behaviour for curved laminates.

4. APPLICATIONS

In this section, the present flow-compaction model is used to predict the compaction of composite laminates manufactured in a production autoclave. In the first case, the laminates were modelled in a similar manner to that in the parametric study (see Figure 8), but a no-slip condition at the tool interface was simulated by imposing displacement constraints at the boundary. Impermeable conditions were maintained at all surfaces except for the top surface of the laminate where the resin pressure was set to the bag pressure. This surface represents the bleeder where the resin is allowed to flow freely during cure. The predicted final shape of the two laminate lay-ups are presented in Figure 17. The laminate lay-up has a significant effect on the deformations at the edge of the laminate. The [0] laminates have small lateral deformations and the tool geometry influences the sign of the shear deformation in the flat section. This behaviour is not observed for the [90] lay-up where the deformation is more important and is



Shear deformation definition

Figure 16. Effect of the fibre bed shear modulus (G_{13}) on the final shear deformation (γ_{13}) distribution in the laminate: (a) SANOM; (b) SAG131; and (c) SAG132

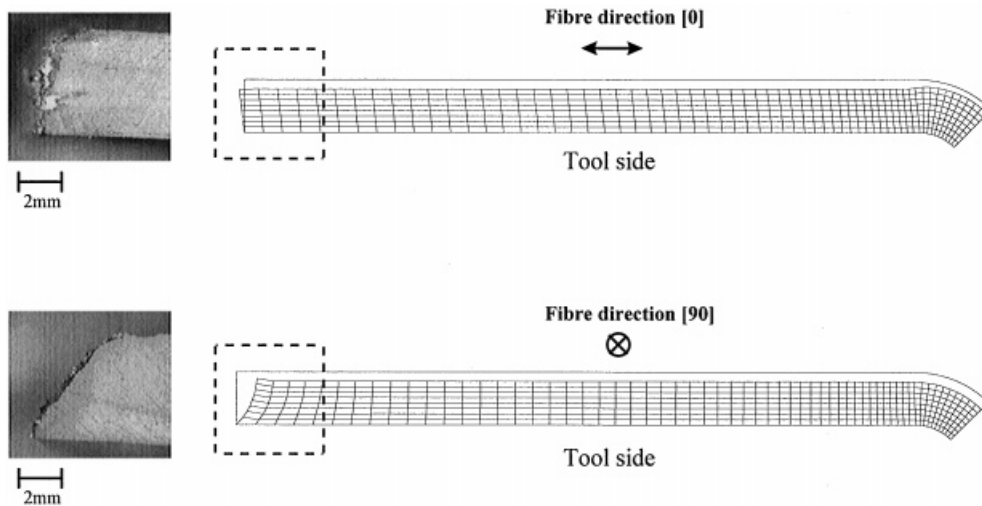


Figure 17. Predicted deformed shape at the end of the compaction for AS4/3501-6 unidirectional laminates [0] and [90]. The original shape of the laminate is shown by the solid line. Photograph of the edge profile of the laminates after cure is also shown

always in the direction of the pressure at the edge. Similar deformation profiles were observed on the actual test specimens as shown in Figure 17. It should be noted that the edges of the laminates were cut square before cure.

In the second case, a specimen moulded on a fairly massive convex tool is considered and therefore both the tool and the laminate were modelled (Figure 18(a)). The cure cycle definition used in the experiment was applied to the model. The appropriate heat transfer coefficient for the autoclave was used, and convection boundary conditions were applied. The temperature profiles predicted by the model are in very good agreement with the measured temperature profiles as shown in Figure 18(b). The compaction strain variation in the flat section (Point A) and at the corner (Point B) are also shown in Figure 18(b). The predicted final compaction strains are in good agreement with the measured final values shown in Figure 18(b).

5. SUMMARY AND CONCLUSIONS

A 2-D plane strain, flow-compaction finite element model has been developed and integrated in a comprehensive model for the autoclave processing of laminated composite structures. A fibre bed constitutive law which assumes a non-linear elastic material behaviour in the fibre transverse direction to the fibre and a linear elastic behaviour in shear has been proposed. Despite its simplicity, the implementation of this new constitutive law in a flow-compaction model shows that:

- The fibre bed shear modulus has a significant influence on the compaction and final shape of curved laminates.
- Accurate measurements of the fibre bed compaction curve and shear behaviour are critical for accurate prediction of the laminate final thickness.

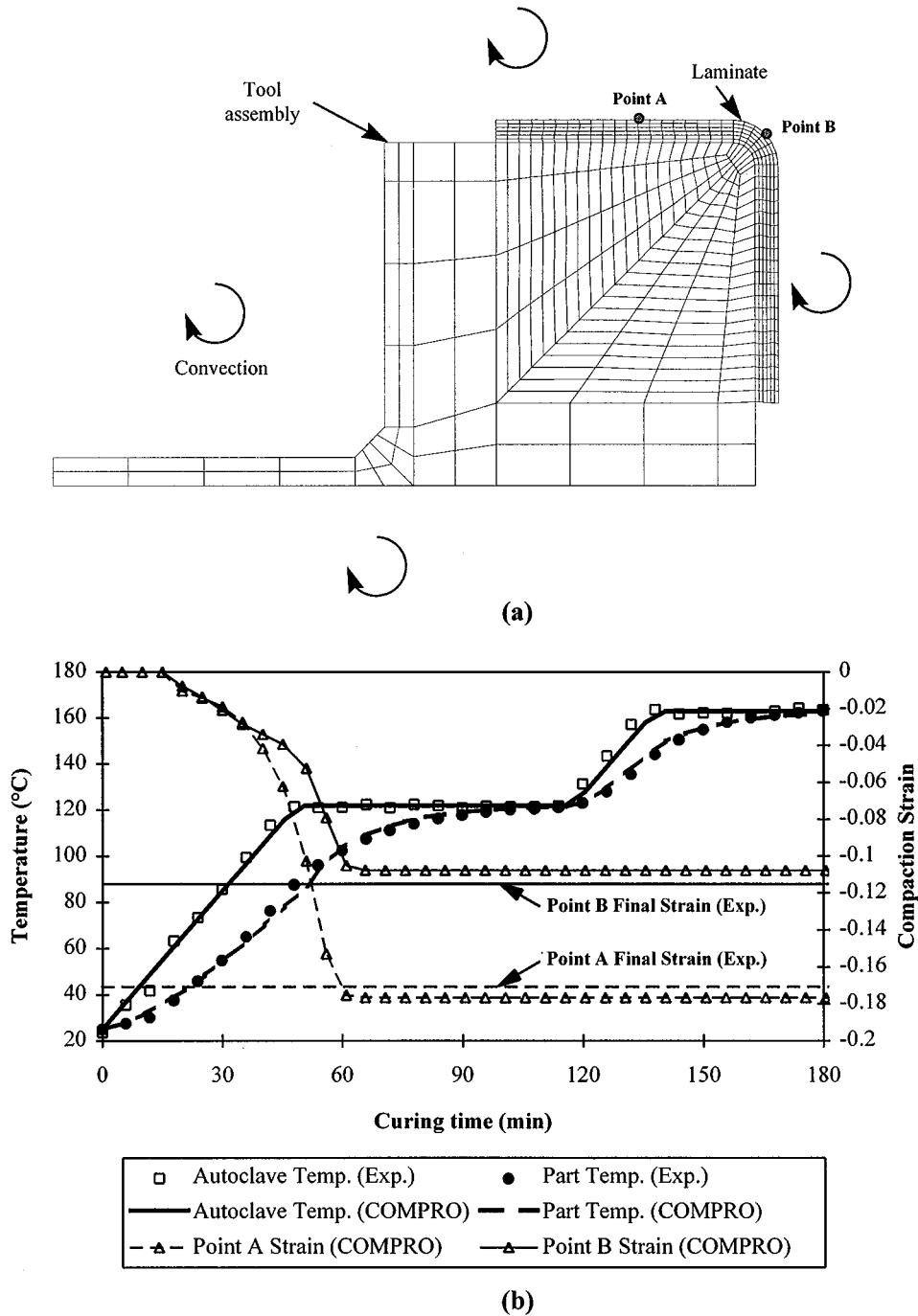


Figure 18. (a) Finite element mesh including the tool and the laminate for a unidirectional AS4/3501-6 composite angle. (b) Temperature profiles and laminate compaction strain predicted by COMPRO compared to the experiments

APPENDIX

Nomenclature

\mathbf{a}^u	displacement degree of freedom
\mathbf{a}^p	resin pressure degree of freedom
\mathbf{B}	shape function derivatives matrix
c	constant for permeability model
\mathbf{C}	damping matrix
\mathbf{D}	stiffness matrix
\mathbf{D}_T	tangent material stiffness matrix
E_1	fibre bed longitudinal modulus
E_3	fibre bed transverse modulus
\mathbf{F}	load vector
\mathbf{F}^{int}	vector of internal loads
\mathbf{F}^g	gravity forces vector
F_i	internal body forces
g	acceleration due to gravity
G_{13}	fibre bed shear modulus
\mathbf{G}	shape function derivatives matrix
h	height above a reference point
\mathbf{H}^d	matrix containing pressure head term
k	Kozeny constant
k'	modified Kozeny constant
K_{ij}	fibre bed permeability tensor
\mathbf{K}	fibre bed permeability matrix
\mathbf{N}	element shape function matrix
P	resin pressure
P_{atm}	atmospheric pressure
P_b	bag pressure
r_f	fibre radius
R	universal gas constant
\mathbf{R}	vector of residual forces
t	time
t_{gel}	time at resin gelation
T	temperature
\dot{u}_i	fibre bed velocity
u^n	displacement normal to the boundary
\mathbf{U}	vector of unknown nodal variables
$\dot{\mathbf{U}}$	vector of time derivatives of the unknown nodal variables
v_i	resin velocity
V'_a	maximum fibre volume fraction for permeability model
V_f	fibre volume fraction
V_f^0	initial fibre volume fraction
α	resin degree of cure
δ_{ij}	Kronecher delta

δ	vector from Kronecher delta
ε_i	fibre bed strain
γ_{13}	fibre bed shear strain
Γ	boundary of the domain
κ	constant for viscosity model
μ	resin viscosity
μ_∞	constant for viscosity model
θ	fibre orientation angle
ρ_R	resin density
σ	autoclave pressure
σ^n	applied traction at the domain boundary
σ_{ij}	total applied stress
$\bar{\sigma}_{ij}$	effective stress
Ω	domain volume

ACKNOWLEDGEMENTS

This work was supported by funding from the Natural Sciences and Engineering Research Council of Canada. We would also like to gratefully acknowledge the significant interaction and support from our colleagues at The University of British Columbia and The Boeing Company.

REFERENCES

1. P. Hubert and A. Poursartip, 'A review of flow and compaction modelling relevant to thermoset matrix laminate processing', *J. Reinf. Plast. Comp.*, **17**(4), 286–318 (1998).
2. A. C. Loos and G. S. Springer, 'Curing of epoxy matrix composites', *J. Comp. Mat.*, **17**, 135–169 (1983).
3. P. Hubert, A. Johnston, R. Vaziri and A. Poursartip, 'A two-dimensional finite element processing model for FRP composite components', *Proc. 10th Int. Conf. on Composite Materials (ICCM-10)*, Whistler, B.C., 1995, pp. 149–156.
4. T. G. Gutowski, T. Morigaki and Z. Cai, 'The consolidation of laminate composites', *J. Comp. Mat.*, **21**, 172–188 (1987).
5. R. Davé, J. L. Kardos and M. P. Dudukovic, 'A model for resin flow during composite processing: Part 1—general mathematical development', *Poly. Comp.*, **8**, 29–38 (1987).
6. G. D. Smith and A. Poursartip, 'A comparison of two resin flow models for laminate Processing', *J. Comp. Mat.*, **27**, 1695–1711 (1993).
7. R. W. Lewis and B. A. Schrefler, *The Finite Element Method in the Deformation and Consolidation of Porous Media*, Wiley, Chichester, 1987.
8. X. Li, O. C. Zienkiewicz and M. Xie, 'A numerical model for immiscible two-phase fluid flow in a porous media and its time domain solution', *Int. J. Numer. Meth. Engng.*, **30**, 1195–1212 (1990).
9. M. V. Brusckhe and S. G. Advani, 'A finite element/control volume approach to mold filling in anisotropic porous media', *Poly. Comp.*, **11**, 398–405 (1990).
10. F. Trochu, R. Gauvin and Z. Zhang, *Computer Aided Design in Composite Material Technology, Vol. III*, Computational Mechanics Publications, Oxford, 1992.
11. W.-B. Young, 'Resin flow analysis in the consolidation of multi-directional laminated composites', *Poly. Comp.*, **16**, 250–257 (1995).
12. C. M. Ó Brádaigh and R. B. Pipes, 'A finite element formulation for highly anisotropic incompressible elastic solids', *Int. J. Numer. Meth. Engng.*, **33**, 1573–1596 (1992).
13. A. K. Pickett, T. Queckborner, P. de Luca and E. Haug, 'Industrial press forming of continuous fibre reinforced thermoplastic sheets and the development of numerical simulation tools', *Proc. 3rd Int. Conf. of the Flow Processes in Composites Materials*, Ireland, 1994, pp. 1–13.
14. ABAQUS, Finite Element Software, © Hibbitt, Karlsson and Sorensen, Inc. 1995.
15. COMPRO, Finite Element Software, © The University of British Columbia, 1997.

16. P. Hubert, 'Aspects of flow and compaction of laminated composite shapes during cure', *Ph.D. Thesis*, The University of British Columbia, Vancouver, 1996.
17. A. Johnston, 'An integrated model of the development of process-induced deformation in autoclave processing of composites structures', *Ph.D. Thesis*, The University of British Columbia, Vancouver, 1997.
18. R. D. Cook, D. S. Malkus and M. E. Plesha, *Concepts and Applications of Finite Element Analysis*, 3rd edn, Wiley, New York, 1989.
19. Z. Cai and T. G. Gutowski, 'The 3-D deformation behavior of lubricated fiber bundles', *J. Comp. Mat.*, **26**, 1207–1237 (1992).
20. O. C. Zienkiewicz and R. L. Taylor, *The Finite Element Method*, McGraw-Hill, London, 1994.
21. J. T. Christian and J. W. Boehmer, 'Plane strain consolidation by finite elements', *J. Soil Mech. Found. Div.*, 1435–1457 (1970).
22. J. Ghaboussi and E. L. Wilson, 'Flow of compressible fluid in porous elastic media', *Int. J. Numer. Meth. Engng.*, **5**, 419–442 (1973).
23. P. A. Vermeer and A. Verruijt, 'An accuracy condition for consolidation by finite elements', *Int. J. Numer. Meth. Engng.*, **5**, 1–14 (1981).
24. O. C. Zienkiewicz, D. K. Paul and A. H. C. Chan, 'Unconditionally stable staggered solution procedure for soil-pore fluid interaction problems', *Int. J. Numer. Meth. Engng.*, **26**, 1039–1055 (1988).
25. G. Dhatt and G. Touzot, *The Finite Element Method Displayed*, Wiley, New York, 1984.
26. D. R. J. Owen and E. Hinton, *Finite Elements in Plasticity*, Pineridge Press Ltd., Swansea, 1980.
27. LAMCURE, Composite Process Modelling Software, © The University of British Columbia, 1992.
28. R. Davé, J. L. Kardos and M. P. Dudukovic, 'A model for resin flow during composite processing: Part 2—numerical analysis for unidirectional graphite/epoxy laminates', *Poly. Comp.*, **8**, 123–132 (1987).
29. T. G. Gutowski, Z. Cai, S. Bauer, D. Boucher, J. Kingery and S. J. Wineman, 'Consolidation experiments for laminate composites', *J. Comp. Mat.*, **21**, 650–669 (1987).
30. B. R. Gebart, 'Permeability of unidirectional reinforcements for RTM', *J. Comp. Mat.*, **26**, 1100–1133 (1992).
31. P. R. Ciriscioli, Q. Wang and G. S. Springer, 'Autoclave curing-comparisons of model and test results', *J. Comp. Mat.*, **26**, 90–102 (1992).